CICE 2023 Rio de Janeiro – Brazil 11TH INTERNATIONAL CONFERENCE ON FRP COMPOSITES IN CIVIL ENGINEERING

SIZE EFFECTS ON MODE I AND MODE II FRACTURE BEHAVIOUR OF COMPOSITE-STEEL BONDED INTERFACE

Jincheng Yang, Delft University of Technology, Netherlands, J.Yang-4@tudelft.nl
Marcio M. Arouche, Delft University of Technology, Netherlands, M.MoreiraArouche@tudelft.nl
Sigurdur Egilsson, Delft University of Technology, Netherlands, S.Egilsson@tudelft.nl
Mathieu Koetsier, Delft University of Technology, Netherlands, M.Koetsier@tudelft.nl
Tjeu Peeters, Delft University of Technology, Netherlands, T.Peeters-1@tudelft.nl
Marko Pavlovic, Delft University of Technology, Netherlands, M.Pavlovic@tudelft.nl

ABSTRACT
Wrapped composite joints offer an innovative alternative to conventional welded joints in steel circular hollow sections (CHS), demonstrating superior performance in ultimate and fatigue limit states. This study experimentally investigates interfacial fracture behaviour between composite and steel in upscaled wrapped composite joints for practical applications. Different-scale composite-steel interface specimens were prepared for Double Cantilever Beam (DCB) and Four-point End Notched Flexure (4ENF) tests to analyze mode I (opening) and mode II (in-plane shear) interfacial behaviour and fracture properties. The findings provide insights into the size effects on composite-steel interfacial behaviour and enhance the modelling of upscaled wrapped composite joints.

KEYWORDS
Wrapped composite joints; interface; bond; weld; CHS; size effects; SERR; DCB; ENF

INTRODUCTION
Wrapped composite joints (Pavlovic et al., 2019) have emerged as a promising alternative to conventional welded joints in steel circular hollow sections (CHS). Recent pilot studies have demonstrated their superior performance in terms of ultimate strength and fatigue resistance (Feng et al., 2022; Feng & Pavlovic, 2021; He et al., 2023; He & Pavlovic, 2022). These wrapped composite joints, using glass fibre reinforced composite to wrap around CHS tubes, offer a competitive and cost-effective solution for various applications, e.g. replacing traditional welded CHS joints in steel jacket supports for offshore wind turbines (Pavlovic, 2021; Topsector Energie, 2021).

However, in order to effectively apply wrapped composite joints in real-world scenarios requiring upscaled sizes, it is crucial to understand the mechanical properties of the composite-steel bonded interface in the joint by taking into account the size effects.

In the work of this paper, an experimental programme was conducted to investigate the size effects on the fracture behaviour of composite-steel interface in wrapped composite joints. Three series of composite-steel interface specimens were prepared in medium-scale (Ms), large-scale (Ls), and full-scale (Fs). These interface specimens were subjected to Double Cantilever Beam (DCB) and Four-point End Notched Flexure (4ENF) tests to evaluate interfacial behaviour in Mode I (opening) and Mode II (in-plane shear), respectively. Digital Image Correlation (DIC) technique was implemented to monitor the deformation of specimens and measure the interfacial crack propagation and crack-tip opening with high accuracy. The test results of the Ms and Ls specimens are introduced and characterized regarding failure mechanism, interfacial cracking, and fracture toughness. By gaining insight into the interfacial behaviour with size effects, the experimental study facilitates the design and application of upscaled wrapped composite joints in practical field scenarios.

EXPERIMENTAL PROGRAMME

Interface specimens and materials

To facilitate the experimental study on size effects, thirty coupons were produced in total for three series of specimens (Ms, Ls, and Fs). Each scale series includes ten specimens, of which five are allocated for DCB tests and the remaining five for 4ENF. Figure 1 illustrates the interface specimens, and the dimensions are outlined in Table 1 for Ms, Ls and Fs respectively.

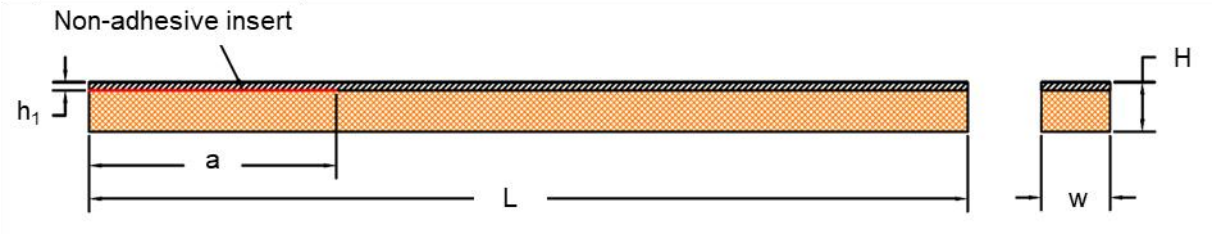

Figure 1: Composite-steel interface specimens prepared for DCB and 4ENF tests

Table 1: Nominal dimensions of interface specimen in Ms, Ls, and Fs

Specimen series	Scale factor	L	a	h_1	w	h
Ms	1	320	90	3.0	25	15
Ls	2	640	180	6.0	50	30
Fs	4	1280	360	12.0	100	60

S355 steel plates with 3, 6 and 12 mm were taken for the manufacturing of the Ms, Ls and Fs specimens, respectively. The bonding surface was pre-treated using grit blasting and degreased prior to the lamination. A non-adhesive insert of 32 µm thickness was placed on the steel plate to induce a pre-cracked region. Then, a vinyl ester resin was applied to the hand lay-up lamination of composite plies. Each composite ply was made of a layer of glass fiber bi-directional woven stitched to a layer of glass fiber chopped strand mat. A total of 12, 24, and 48 plies were laminated to manufacture the Ms, Ls and Fs specimens, respectively. The laminated plates were allowed to cure at room conditions. Finally, steel-composite plates were cut to 0/90 coupon specimens of a predefined geometry.

For the bi-material configuration, the thicknesses of steel and composite adherents are designed to meet the criterion of strain equivalence, as described in Eq. 1, such that the two arms have the same longitudinal strain at the faying surfaces to obtain a pure mode I loading condition (Arouche et al. 2019):

$$E_1 h_1^2 = E_2 h_2^2 \qquad \text{Eq. 1}$$

Where E_1, h_1, E_2 and h_2 are the flexural modulus and thickness of the upper and lower arms, respectively. It is important to notice that the actual thickness of the specimens deviate due to uncertainties of the manufacturing process.

Test setup and measurement

DCB tests

For the specimens in DCB tests, two loading blocks were adhesively attached to both the steel and composite parts. These blocks were connected to a hydraulic jack on the upper and lower sides through pin connections. On the other end of the specimen, a counterweight was applied through a pulley over the specimen to balance the self-weight of the specimen and then reduce the mode mixity induced by asymmetric loading. Figure 2 illustrates the specimen subjected to DCB test configuration. To ensure consistent loading conditions, the load was applied at a constant displacement rate of 1.0 mm/min, 1.5 mm/min, and 2.0 mm/min for the Ms, Ls, and Fs specimens, respectively. The applied load was measured by calibrated load cells and recorded at a frequency of 1 Hz.

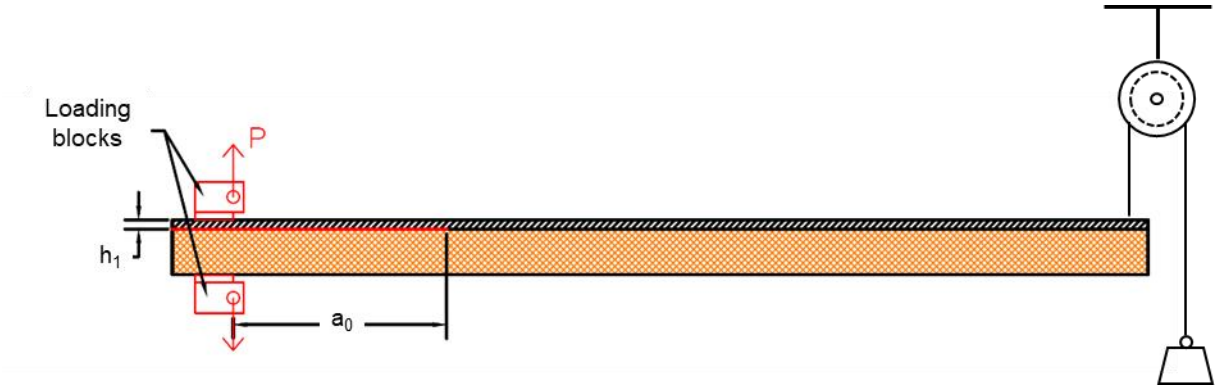

Figure 2: Interface specimen subjected to DCB tests (see dimensions in Table 2)

4ENF tests

The specimen in 4ENF test configuration is illustrated in Figure 3. Same as the DIC tests, the load in 4ENF testes was applied at a constant displacement rate of 1.0 mm/min, 1.5 mm/min, and 2.0 mm/min for the Ms, Ls, and Fs specimens, respectively. The applied load was measured by calibrated load cells and recorded at a frequency of 2 Hz.

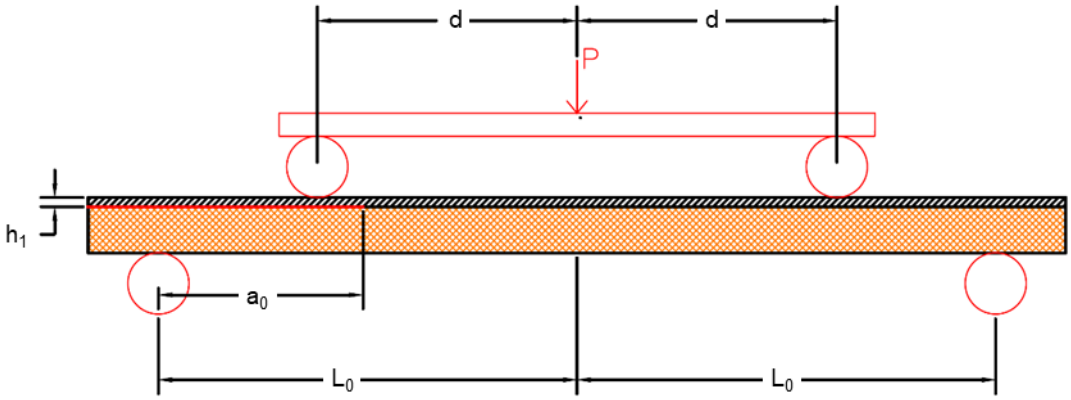

Figure 3: Interface specimen subjected to 4ENF tests (see dimensions in Table 2)

Table 2: Dimensions of interface specimens in DCB test setup

Group	DCB	4ENF		
	a_0	L_0	D	a_0
Ms	67	137	85	67
Ls	134	274	170	134
Fs	268	548	340	268

Digital Image Correlation (DIC)

DIC technique was implemented to monitor both DCB and 4ENF tests. To facilitate DIC measurements, all specimens were coated on one side with suitable black-white speckle patterns. The DIC cameras were configured to capture images at a frequency of 1/5 Hz for the DCB tests and 1/3 Hz for the 4ENF tests. Additionally, polarized blue light was directed onto the specimen surface to establish a stable illumination environment for accurate measurements. The images acquired by the DIC systems were processed using the GOM software package (GOM Correlate Pro) to visualize and monitor the deformation of the specimens within the measurement volume.

RESULTS AND DISCUSSION

In the present study, the results of Ms and Ls interface specimens were preliminarily processed and compared for investigation, including load-displacement relationship, interfacial cracking, and strain energy release rate for R-curves.

DCB tests

Load and displacement

In Figure 4, the displacement of the loading points in response to the applied load is depicted for the medium-scale (Ms) and large-scale (Ls) specimens during the DCB tests. All five Ms specimens were tested and exhibited peak forces ranging from 230 N to 356 N. Three Ls specimens were tested, showing peak forces ranging from 960 N to 1008 N with a limited deviation of 4%.

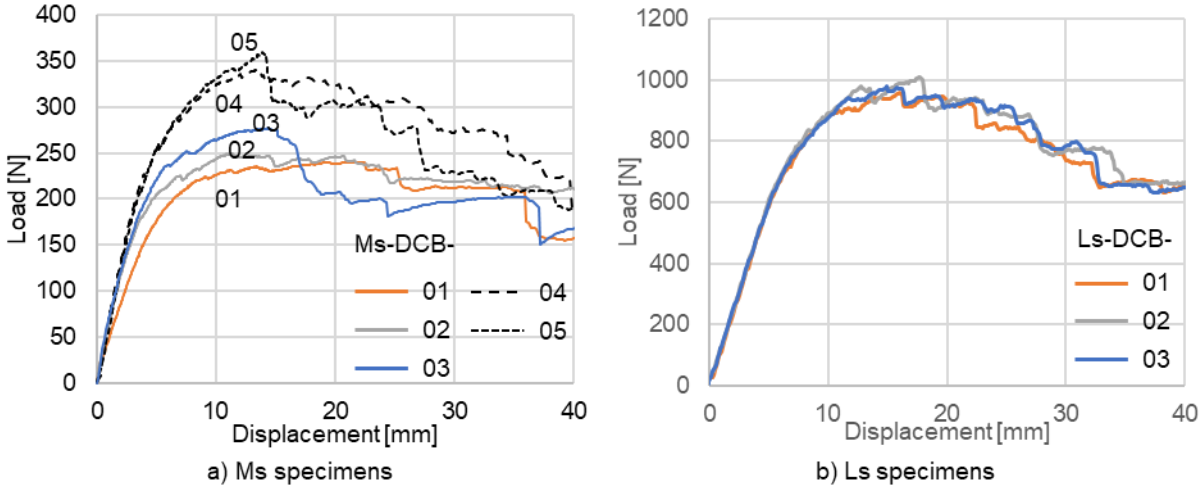

Figure 4: Load-displacement curves of interface specimens in DCB tests

Notably, the load and displacement diagram of the Ms specimens displayed a significantly higher scattering behaviour compared to that of the Ls specimens. It is worth noting that the load and displacement diagram of the Ms specimens exhibited a higher degree of scattering compared to that of the Ls specimens. This scattering behavior in the Ms specimens may be attributed to variations in surface preparation and specimen manufacturing. The difference in interfacial bond quality was revealed by different degree of fiber bridges observed during the tests. Figure 5 presents images of the five Ms specimens captured at a similar opening displacement of the loading points. The images provide a comparison of the fiber bridging. It is evident that specimens Ms-DCB-04 and 05, which exhibit more pronounced fiber bridging, achieved higher peak forces, approximately 40% higher than the average peak force of the remaining three specimens (Ms-DCB-01, 02, and 03).

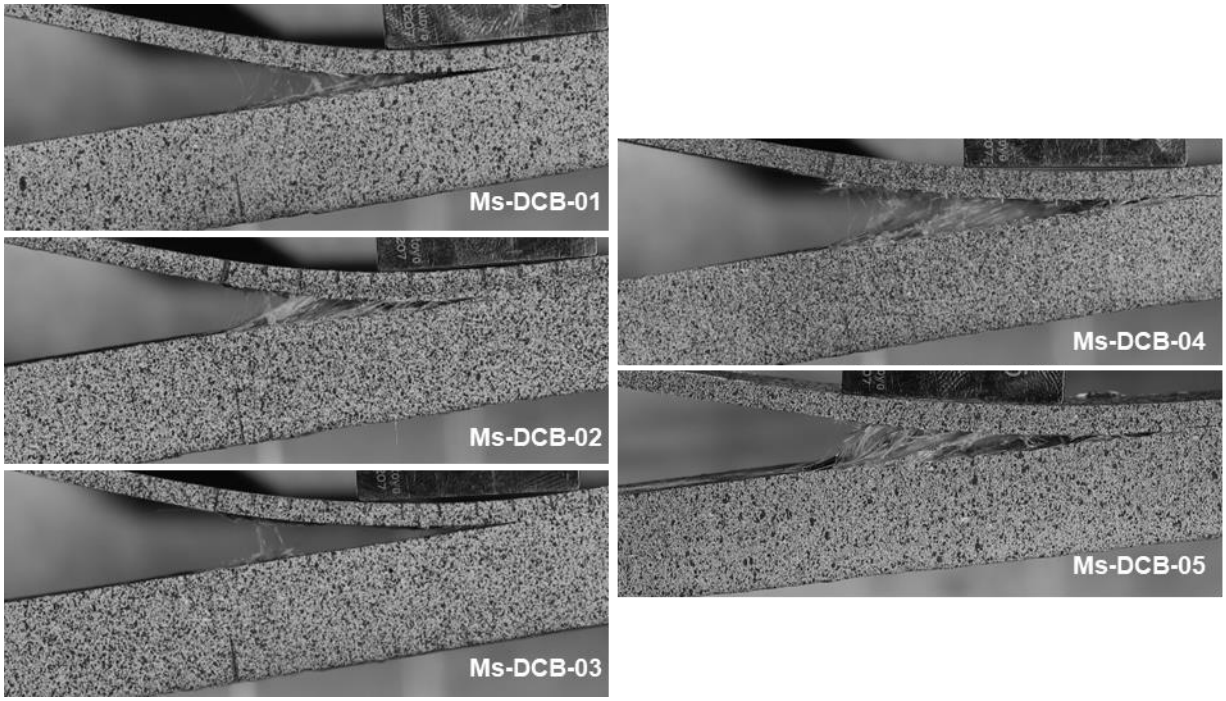

Figure 5: Fiber bridges observed in Ms specimens in DCB tests

Development of interfacial cracking

The deformation between the composite and steel parts of interface specimens was analyzed using Digital Image Correlation (DIC) technique. Figure 6 shows one of the images of an Ls specimen taken by the DIC system. After postprocessing, it allows the measurement of opening displacement along the bond interface. By setting an appropriate threshold value, the location of the crack tip at different stages could be determined.

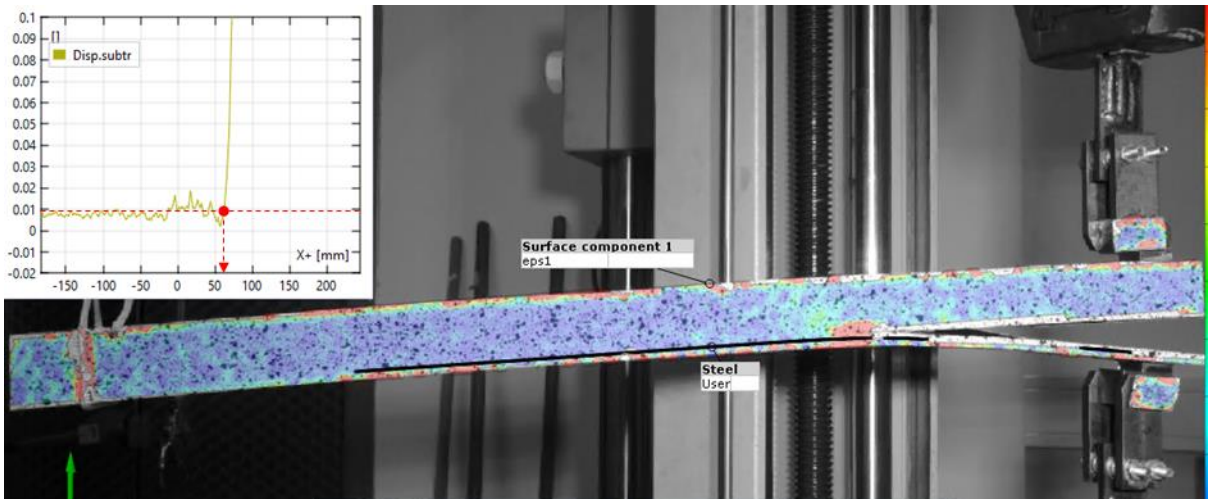

Figure 6: Identify the location of the crack tip in an Ls-DCB specimen based on DIC-acquired data

The DIC technique enables the observation of the initiation and development of interfacial cracks during the loading process. Figure 7 depicts the increasing interfacial crack length in the DCB tests of both Ms and Ls specimens.

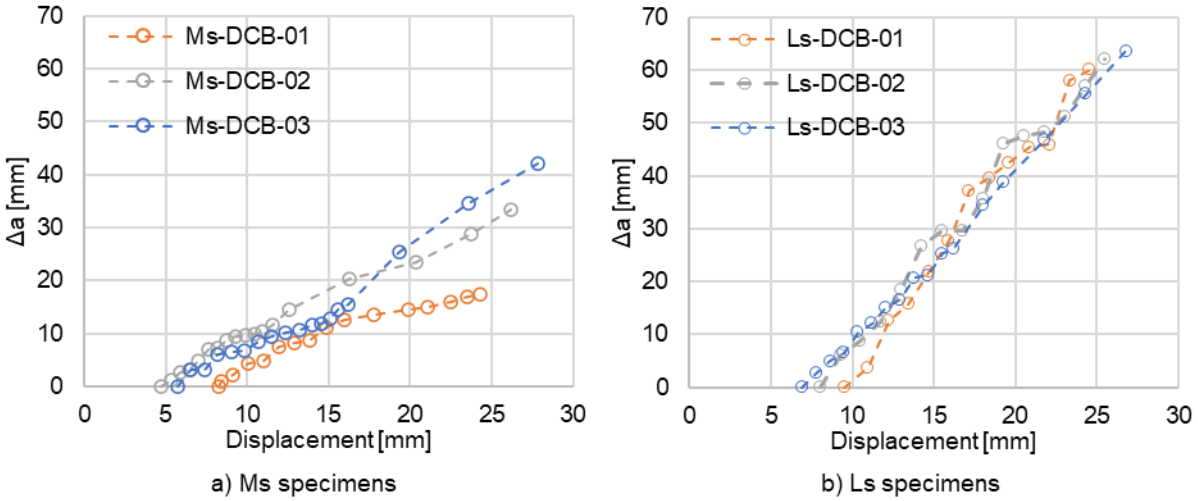

Figure 7: Increased crack length the DCB tests of Ms and Ls specimens

R-curves for Mode I

Given the estimated crack growth at each stage, the corresponding strain energy release rate (SERR) was calculated by extended global method (EGM) (Shahverdi et al., 2014). Figure 8 illustrates the evolution of SERR values as the interfacial crack length increases in the DCB tests of Ms and Ls specimens.

In the Ms specimen, the SERR in Mode I (G_I) reached a plateau value of 0.9 N/mm when the fracture process zone was fully developed. However, the Ls specimen exhibits a higher plateau value of G_I, reaching 1.8 N/mm. It is important to note that the difference in the plateau value of G_I between the Ms and Ls specimens may be magnified by the scattering results observed in the Ms specimens.

Considering the fact that the other two Ms specimens (Ms-DCB-04/05) demonstrated 40% higher loads compared to the three processed specimens (Ms-DCB-01/02/03) shown in Figure 4, a preliminary estimation suggests that the plateau G_I values for Ms-DCB-04/05 could be 96% higher, which aligns with the values estimated in the Ls specimens. It is important to verify this estimation after further postprocessing of the remaining two Ms specimens.

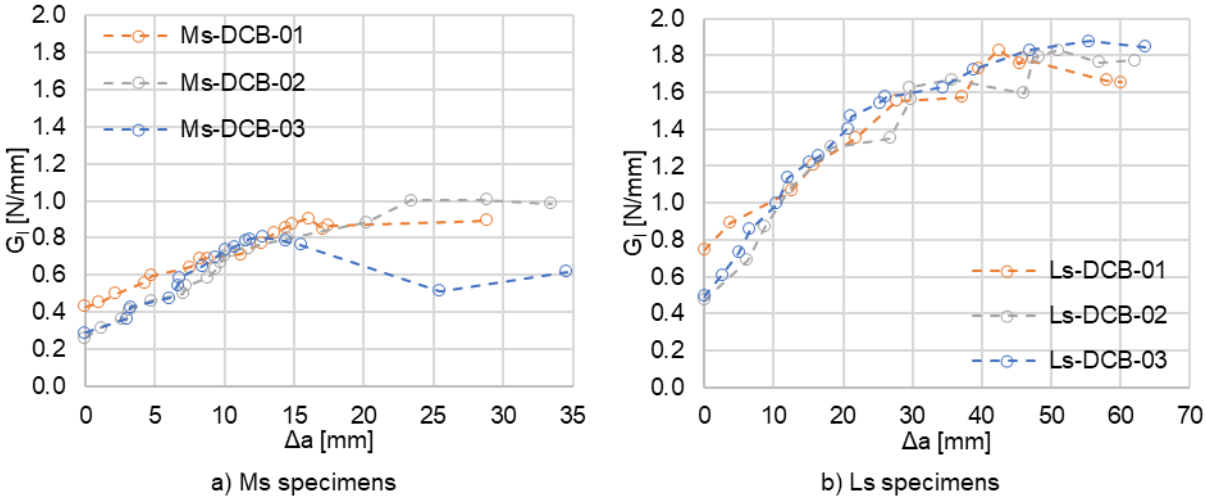

Figure 8: SERR in Mode I (G_I) with the increase of crack length (R-curves)

4ENF tests

Load and displacement

In the 4ENF tests, the displacement was calculated as the net displacement between two loading points and two supports. Figure 9 shows the net displacement of Ms and Ls specimens with the increase of

applied load during the 4ENF tests. Both Ms and Ls specimens exhibit consistent peak force with a deviation within approximately 10%.

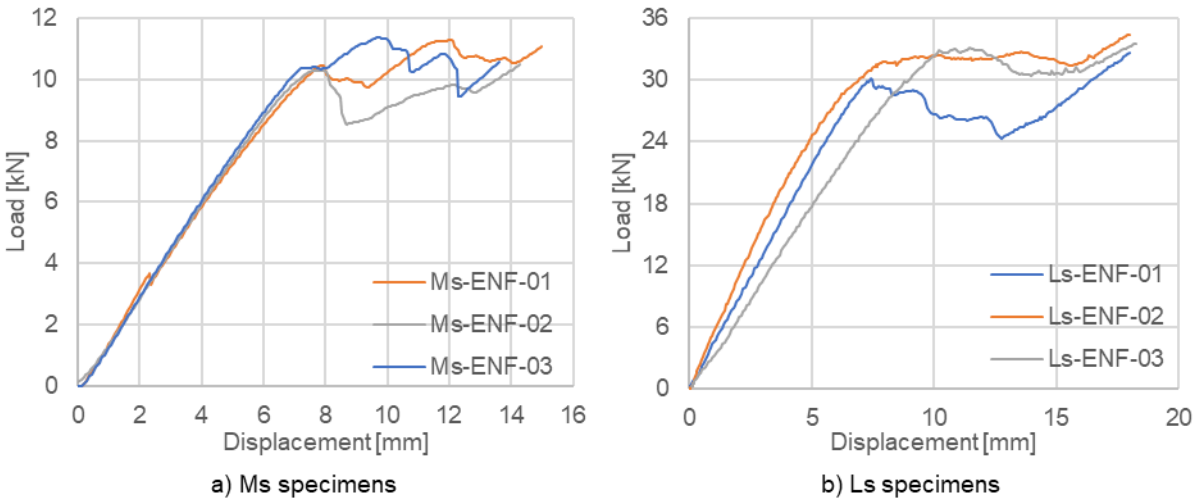

Figure 9: Load-displacement curves of interface specimens in 4ENF tests

Development of interfacial cracking

For the specimens in 4ENF tests, the local deformation of in-plane shear along the bond line was accurately assessed by utilizing DIC measurement. Figure 10 illustrates the approach to identifying the location of the crack tip based on the shear strain distribution along the interface curve and a properly defined threshold. The interfacial crack initiation and propagation were estimated for Ms and Ls specimens in 4ENF tests, as shown in Figure 11.

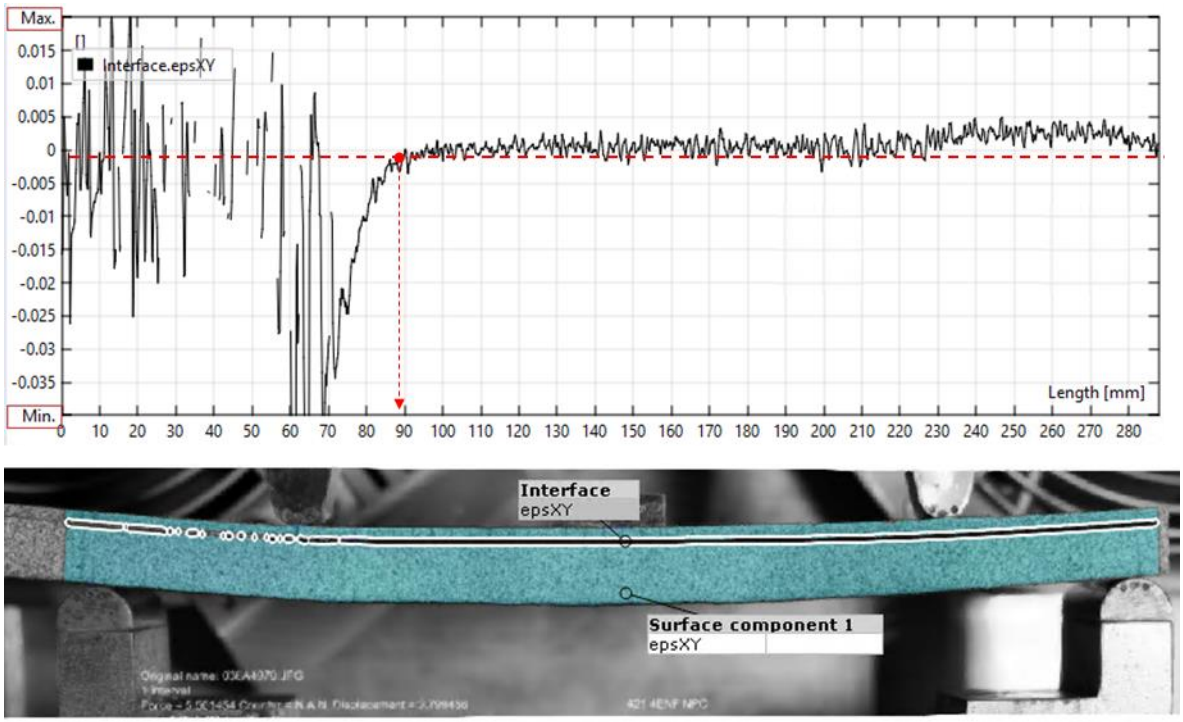

Figure 10: Identify the location of the crack tip in an Ms-4ENF specimen based on DIC-acquired data

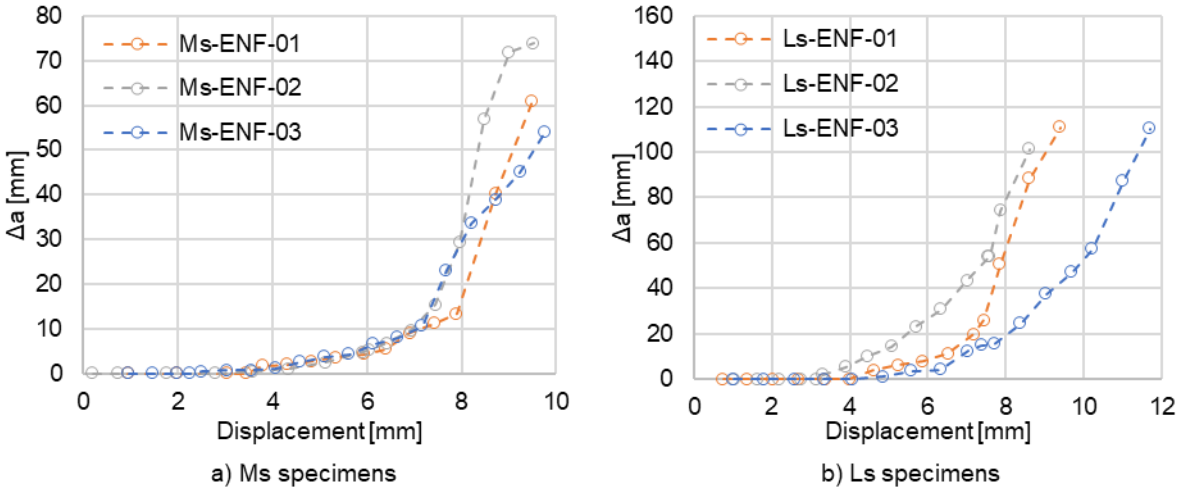

Figure 11: Increased crack length the 4ENF tests of Ms and Ls specimens

R-curves for Mode II

The SERR values in Mode II was evaluated extended global method (Shahverdi et al., 2014). Figure 12 presents the progression of SERR values as the interfacial crack length increases throughout the 4ENF tests performed on Ms and Ls specimens. For the Ms specimen, the Mode II SERR (G_{II}) demonstrated an average plateau value of approximately 8 N/mm. In contrast, the Ls specimens exhibited a higher plateau range for G_{II}, varying between 12 and 14 N/mm. The observed difference in G_{II} plateau values between the Ms and Ls specimens requires further investigation to comprehend the underlying factors contributing to this distinction. In conjunction with this analysis, it would be of interest to examine the R-curves of the Fs specimens to facilitate the investigation of size effects.

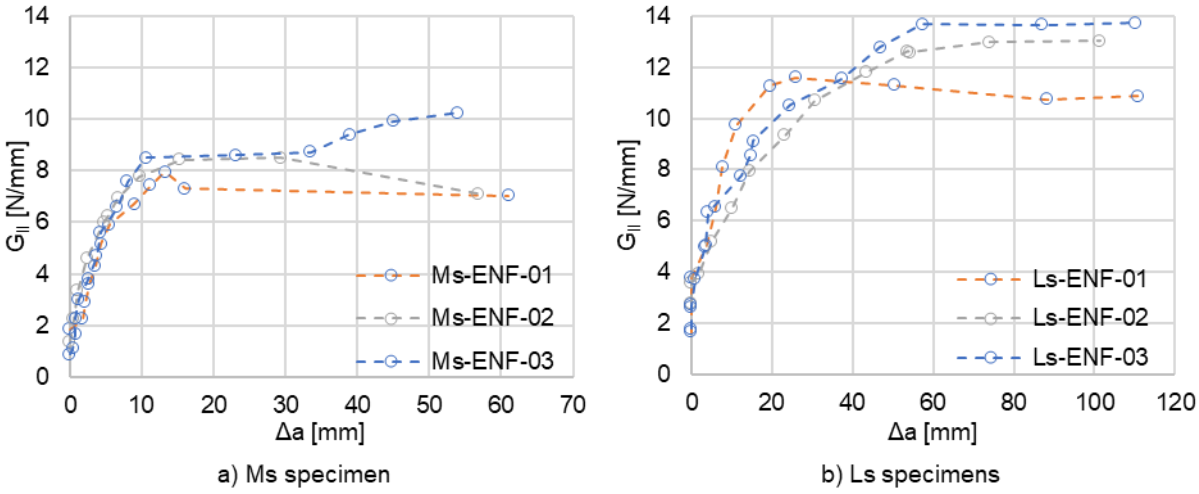

Figure 12: SERR in Mode II (G_{II}) with the increase of crack length (R-curves)

CONCLUSIONS AND FUTURE OUTLOOK

The current study focused on experimental investigations of fracture properties in composite-steel interfaces of innovative wrapped composite joints, with a specific emphasis on size effects in both Mode I and Mode II. Based on the obtained experimental results and observations, the following conclusions can be drawn:

- The utilization of the DIC technique proved to be a powerful and effective tool for capturing interfacial behaviour and key aspects such as crack tip opening displacement. Its high accuracy and reliability make it a valuable asset in similar studies of bi-material interface specimens.
- The size increase from medium-scale (Ms) to large-scale (Ls) specimens displayed a notable reduction in scattering behaviour and a more consistent display of interfacial properties, as

evident in the load-deflection diagram and R-curves obtained from the DCB tests of Ls specimens.

- To further explore the variation in interfacial properties in Mode II and identify the underlying factors contributing to the differences in R-curves, the remaining test results of Ms and Ls specimens should be processed and analyzed further to enhance the understanding of the observed variations.
- To gain a comprehensive understanding of the interfacial properties and their size effects, it is crucial to incorporate Fs specimens into the processing and analysis alongside Ms and Ls specimens. This will enable a holistic examination of the composite-steel interfaces across different sizes, contributing to a more thorough comprehension of the size effects.

Additionally, to validate the experimental findings concerning the size effects on composite-steel interfacial behaviour, future studies will involve the implementation of nonlinear finite element modelling. This computational approach will serve to further validate and enhance our understanding of the observed experimental results.

By addressing these future studies, it enhances the understanding of the fracture properties and size effects in composite-steel interfaces, paving the way for modelling and optimal design of wrapped composite joints in practical applications.

ACKNOWLEDGEMENT
The authors would like to express their gratitude to RVO for the financial support with Topsector Energiesubsidie van het Ministerie van Economische Zaken through WrapNode-I project, and Tree Composites B.V. for the production of specimens.

CONFLICT OF INTEREST
The authors declare that they have no conflicts of interest associated with the work presented in this paper.

DATA AVAILABILITY
Data on which this paper is based is available from the authors upon reasonable request.

REFERENCES

Feng, W., He, P., & Pavlovic, M. (2022). Combined DIC and FEA method for analysing debonding crack propagation in fatigue experiments on wrapped composite joints. *Composite Structures*, *297*, 115977. https://doi.org/10.1016/J.COMPSTRUCT.2022.115977

Feng, W., & Pavlovic, M. (2021). Fatigue behaviour of non-welded wrapped composite joints for steel hollow sections in axial load experiments. *Engineering Structures*, *249*. https://doi.org/10.1016/J.ENGSTRUCT.2021.113369

He, P., Feng, W., & Pavlovic, M. (2023). Influence of steel yielding and resin toughness on debonding of wrapped composite joints. *Composite Structures*, *312*, 116862. https://doi.org/10.1016/J.COMPSTRUCT.2023.116862

He, P., & Pavlovic, M. (2022). Failure modes of bonded wrapped composite joints for steel circular hollow sections in ultimate load experiments. *Engineering Structures*, *254*, 113799. https://doi.org/10.1016/J.ENGSTRUCT.2021.113799

Pavlovic, M. (2021). *Wrapped Composite Joints for Next Generation Offshore wind support structures - Phase 1 (WrapNode-I)*. 2021. https://grow-offshorewind.nl/project/wrapnode

Pavlovic, M., Veljkovic, M., & Bogers, P. (2019). *Method for making a virgin joint between two separate structural hollow sections, and such a virgin joint*. https://research.tudelft.nl/en/publications/method-for-making-a-virgin-joint-between-two-separate-structural-

Shahverdi, M., Vassilopoulos, A. P., & Keller, T. (2014). Mixed-Mode I/II fracture behavior of asymmetric adhesively-bonded pultruded composite joints. *Engineering Fracture Mechanics*, *115*, 43–59. https://doi.org/10.1016/J.ENGFRACMECH.2013.11.014

Topsector Energie. (n.d.). *Wrapped Composite Joints for Next Gen Offshore wind support struc. (WrapNode-I)* . Retrieved June 1, 2023, from https://projecten.topsectorenergie.nl/projecten/wrapped-composite-joints-for-next-gen-offshore-wind-support-struc-wrapnode-i-35837